ACS APPLIED MATERIALS & INTERFACES

Research Article

www.acsami.org

Waterborne Polyurethanes with Tunable Fluorescence and Room-Temperature Phosphorescence

Cao Zhou,[†] Tongqing Xie,[†] Rui Zhou,[†] Carl O. Trindle,[‡] Yavuz Tikman,[§] Xingyuan Zhang,*[,†] and Guoqing Zhang*[,†]

[†]CAS Key Laboratory of Soft Matter Chemistry, Department of Polymer Science and Engineering, University of Science and Technology of China, Hefei, 230026 China

[‡]Department of Chemistry, University of Virginia, McCormick Road, Charlottesville, Virginia 22904, United States

[§]Physics Department, Marmara University, Göztepe Kampus, 34722 Kadiköy Istanbul, Turkey

Supporting Information

ABSTRACT: Single-component materials with both fluorescence and room-temperature phosphorescence (RTP) are useful for ratiometric sensing and imaging applications. On the basis of a general design principle, an amino-substituted benzophenone is covalently incorporated into waterborne polyurethanes (WPU) and results in fluorescence and RTP single-component dual-emissive materials (SDMs). At different aminobenzophenone concentrations, the statistical, thermal, and optical properties of these SDMs are characterized. Despite their similar thermal behaviors, the luminescence properties as a function of the chromophore concentration are quite different: increasing concentrations led to progressively narrowed singlet−triplet energy gaps. The tunability of fluorescence and RTP via chromophore concentration is explained by a previously proposed model, polymerization-enhanced intersystem crossing (PEX). The proposal of PEX is based on Kasha's molecular exciton theory with a specific application in polymeric systems, where the polymerization of luminophores results in excitonic coupling and enhanced forward and reverse intersystem crossing. The mechanism of PEX is also examined by theoretical calculations for the WPU system. It is found that the presence of **K1** aggregates indeed enhances the crossover from singlet excited states to triplet ones.

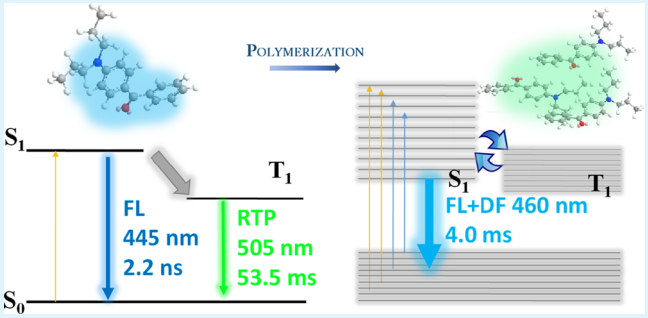

KEYWORDS: *fluorescence, room-temperature phosphorescence, single-component, dual-emissive, waterborne polyurethane*

INTRODUCTION

Materials with both fluorescence and room-temperature phosphorescence (RTP)[1,2] have been successfully used in sensing and imaging applications.[3−5] In a previous study, we proposed a general design strategy for synthesizing aromatic-ketone based single-component, dual emissive materials (SDMs).[6] A key process in the design is to use charge-transfer (CT) states to facilitate the communication between $n-\pi^*$ and $\pi-\pi^*$ states of aromatic ketones. The small CT-induced singlet−triplet energy gap (ΔE_{ST}) has been shown to increase the intersystem crossing (ISC) efficiency, which ultimately results in strong RTP, in addition to the intense CT fluorescence. The strategy has proven conducive to generating dual-emissive materials and has found applications in optical sensing for molecular oxygen, a good RTP quencher.[7,8] A recent review by Wolfbeis[9] et al. has many great examples on oxygen sensing with various RTP materials.

In order to effectively harness RTP for these aromatic carbonyl dyes, they have to be incorporated into rigid matrices such as polymers[4,8,10] with good optical transparency or crystals.[11−14] The dyes can either be blended into[10,15] or covalently attached[4,16] to the polymer matrices via a variety of methods. The former is less synthetically challenging but could pose problems when the dye concentrations are so high that phase separation may occur. Furthermore, blending also requires that the dye and polymer be thoroughly dissolved in a solvent first before the solution evaporates to give a homogeneous mixture. The latter method of chemically linking dyes and polymers can effectively address these issues. For example, Fraser et al.[17−20] developed a series of dual-emissive dye-initiators used for the ring-opening polymerization of lactones and the resulting dye-modified polyesters show enhanced photophysical properties. These biocompatible polymers are fabricated into nanosensors to successfully image oxygen distribution in vivo within a solid tumor.[4] Nonetheless, the main limitation of dye-initiation is that very few types of chemistry can be achieved. For example, dye-initiation is mostly used to generate end-functionalized

Received: May 11, 2015
Accepted: July 20, 2015
Published: July 20, 2015

DOI: 10.1021/acsami.5b04075
ACS Appl. Mater. Interfaces 2015, 7, 17209−17216

Scheme 1. Preparation of Single-Component Dual-Emissive Materials (SDMs) from a Waterborne Polyurethane[a]

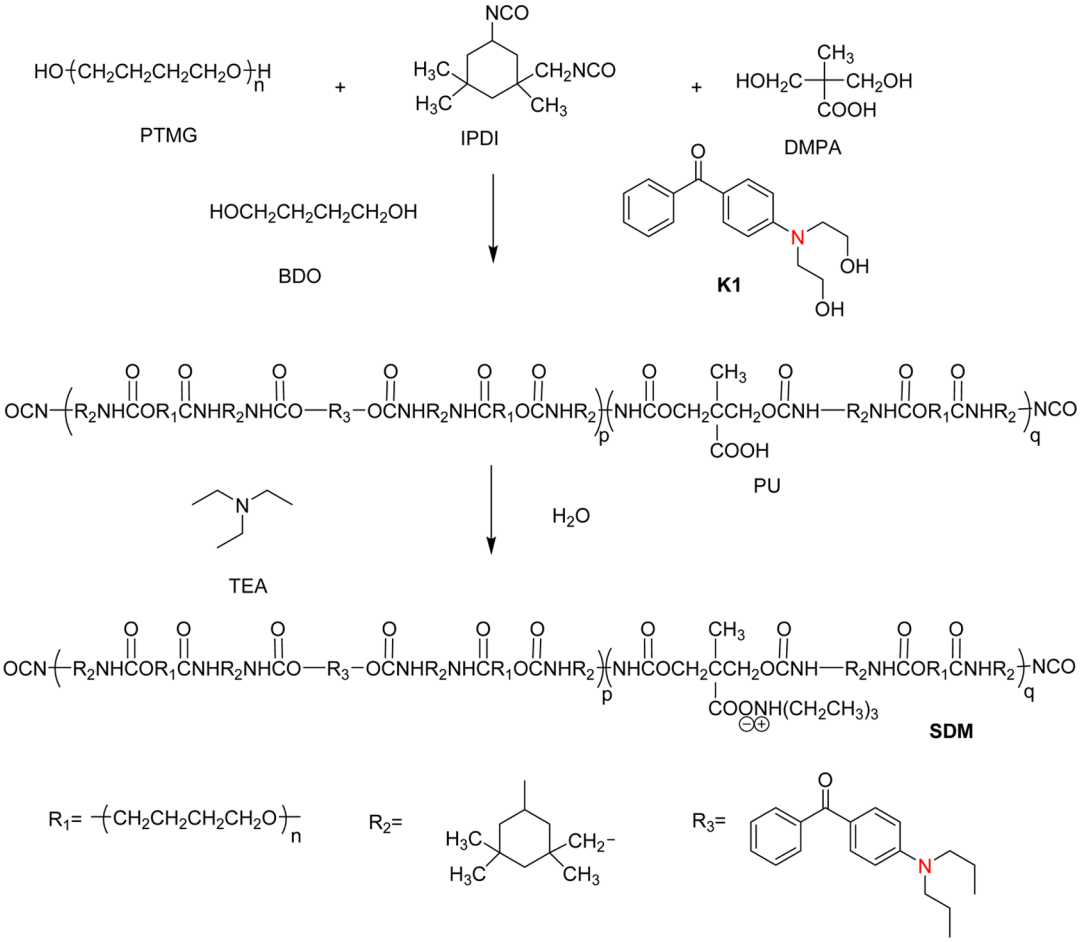

[a]For abbreviations please refer to the Supporting Information, SI.

polymers and is prone to the aggregation effect. End-functional fluorophores are also more susceptible to thermal quenching compared to the main-chain type due to increased free volumes.[20] Furthermore, the polymer molecular weight has to be small in order to achieve high dye concentrations, which may compromise the thermal and mechanical properties from the low molecular weights. RTP dyes have also been made into monomers[21] or attached to the polymers via postpolymerization modifications.[22] However, there is virtually no report on integrating RTP dyes as a component into polycondensation reactions by which many industrial polymers are prepared. In general, polycondensation requires less stringent reaction conditions (vs chain reactions that constantly needs catalysts and a water/oxygen-free environment) and can generate polymers with much larger molecular weights for the same type of monomers. This method enables us to expand SDM studies to entirely different classes of polymers and may also allow for high dye loadings without phase-separation or sacrifice of molecular weights. In addition, the dual-emissive comonomer luminophore is easily prepared for polycondensation reactions since it contains two hydroxyl groups.

Here, we present our latest work to use environmentally friendly and biocompatible waterborne polyurethanes[23−25] (WPUs, Scheme 1) as a suitable medium to produce SDMs. WPUs are a class of highly versatile polymeric materials that have been widely used as paints, coatings, foams, elastomers, and thermoplastics because of their many possibilities in the selection of monomers; we expect that luminescent dyes can be easily incorporated into WPUs with minimal modifications. In additional, the dye aggregation problem can be minimized. The dual-emissive aromatic ketone selected in this study is *N,N*-hydroxyethylamino benzophenone (**K1**) which is stable in aqueous and ambient conditions, whereas previous boron dyes have shown partial degradation over time.[26,27] The synthesis and optical characterization of WPUs containing different ratios of **K1** will serve as the main focus of this initial report: we found that the dual emission from these WPUs can be affected by **K1** concentrations, which is very well explained by a model[16,28] we recently proposed.

RESULTS AND DISCUSSION

The dual-emissive dye monomer **K1** (Scheme 1) was synthesized from the reaction of 4-chlorobenzophenone and diethanolamine in the presence of KOH at 130 °C. The subsequent procedure for obtaining **K1**-containing WPUs is illustrated in Scheme 1. Similar experimental conditions have been previously reported to generate other functional WPUs;[29] briefly, two major steps include chain extension and emulsification. Different aliquots of **K1** were added in the first step (Table 1) while the rest of the reactants were kept unchanged, after which a prepolymer bearing −COOH side groups was obtained. Triethylamine was then added to form ammonium carboxylate salts which serve as internal emulsifiers in an aqueous solution. Dynamic light scattering (DLS) shows

DOI: 10.1021/acsami.5b04075
ACS Appl. Mater. Interfaces 2015, 7, 17209−17216

Table 1. GPC Characterization of SDM Films of Varying K1 Content

polymer[a]	BDO:K_1[b]	wt %[c]	M_n[d]	PDI[e]
SDM0	3.46:0.00	0	14900	1.85
SDM1	3.31:0.15:	1	50000	3.69
SDM2	3.16:0.29	2	46200	2.99
SDM5	2.71:0.75	5	61300	4.20
SDM10	1.90:1.55	10	24000	2.74
SDM20	0.00:3.46	20	17700	2.42

[a]All polymer samples were synthesized at the PTMG:IPDI:DMPA ratio of 1:7:1.86. Measurements were performed for redissolved SDM films in THF. [b]Molar ratio by setting PTMG = 1. [c]Weight percentage of **K1** in the reactants. [d]Number-average molecular weight measured in THF at 40 °C. [e]Polydispersity index (PDI = M_w/M_n).

highly reproducible average radii of ∼20−35 nm (Figure S1) for these WPUs. The latex of each WPU was then allowed to dry under an infrared light over the course of 5−10 min and formed a clear film.

The polyurethane (PU) polymers prior to emulsification were characterized by gel-permeation chromatography (GPC, Table 1, note that the molecular weight information for WPUs is not considered as reliable from GPC, most likely due to the presence of extremely polar carboxylate and ammonium groups). The polymers in all cases exhibit broad molecular-weight distributions (PDI = 1.85−4.20) typical of poly-condensation reactions. Shown in Figure 1 are the IR spectra

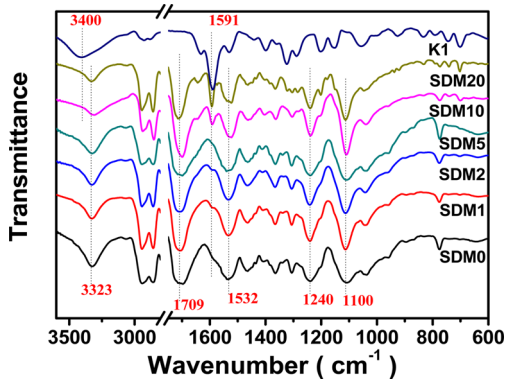

Figure 1. Infrared (IR) transmission spectra of SDM films with various **K1** contents on KBr plates.

of the SDM films with the number denoting the weight percentage of **K1** (e.g., 5% **K1** by weight = **SDM5**). Compared to the pure **K1** solid film, the characteristic O−H vibration at 3400 cm^{-1} is absent for all the SDM films, suggesting that **K1** is chemically linked to the polymer chains. The peaks at 3323 and 1709 cm^{-1} are assigned as the stretching motions of N−H and C═O from the carbamate group. Peak assignment for SDM films:[30] 3323 cm^{-1} [ν(NH)], 2856−2949 cm^{-1} [$\nu(CH_2)$ and $\nu(CH_3)$], 1709 cm^{-1} [ν(C═O)], 1532 cm^{-1} [δ(N−H)], 1240 cm^{-1} [ν(−C-O) of carbamate group], and 1110 cm^{-1} [ν(C−O−C)]. The characteristic absorption peaks corresponding to **K1** could be observed clearly at 1591 cm^{-1} [ν(C═O)] indicative of the aromatic carbonyl structure.

Figure 2 shows the thermal behaviors of the SDM films. From the differential scanning calorimetry (DSC) data, all samples exhibit a broad endothermic peak in the range of 50−70 °C, which is not a typical glass transition but might be due to the disruption of ordered structures in the hard segments.[31]

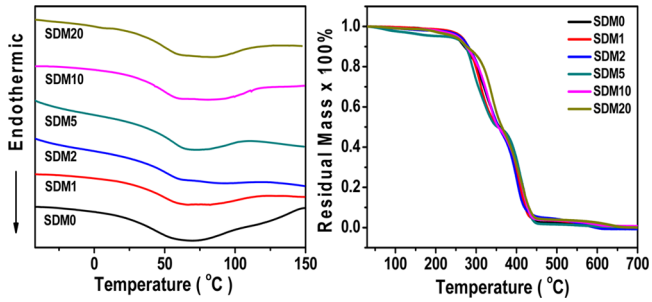

Figure 2. Thermal characterization of SDM films with various **K1** contents via DSC (a) and TG (b) measurements.

Nonetheless, comparing to the sample that does not contain **K1** at all (i.e., **SDM0**), with increasing **K1** content in the SDMs, the peak maxima are lowered by ∼3−5 °C. The decrease is most likely due to the plasticizing effects from the bulky pendant **K1** molecules, which can disrupt the intermolecular interactions among the polymer chains. From thermogravimetry (TG) analysis, all films show descending slopes from the onset due to losses of small molecules such as water and/or triethylamine. It seems that the curve for **SDM20** has a slightly late appearance in the 250−350 °C region where carbamate bonds start to break.

The luminescence properties of the SDMs are then investigated mainly in the solid state, because they mostly likely find applications in solid state. When excited with UV light (λ_{ex} = 396 nm), the crushed crystalline powder of **K1** exhibits moderately strong (Φ_{solid} = 0.051) emission at 507 nm (Figure 3a) with a pre-exponent-weighted lifetime[4] of 0.76 ns. This forms a huge contrast with the luminescence emission of benzophenone (BP) the photophysical properties of which have been well-documented in the solid state.[12] The emission of BP is blue-shifted (λ_{em} = 449 nm) and very structured with a lifetime of 316.5 μs. The vibronic spacing of the emission spectrum is ∼1540 cm^{-1}, which indicates that the luminescence originates from the carbonyl-localized triplet $n-\pi^*$ transition. With the presence of a strong electron-donating dialkylamino group in the π-conjugated system, the vibronic structure completely disappears, most likely due to the fact that the lowest electronic transition state is dominated by the singlet $\pi-\pi^*$ with a CT nature.[6,32]

After **K1** is incorporated into the polymer at a 1% weight ratio, the emission spectra of the **SDM1** emulsion (λ_{em} = 448 nm) and dried film (λ_{em} = 445 nm) under air at room temperature are very similar except that the emulsion spectrum is slightly broadened, presumably due to its more heterogeneous environment (Figure 3a). The fluorescence quantum yields in air ($\Phi_{emul,SDM1}$ = 0.12, relative to quinine sulfate and $\Phi_{film,SDM1}$ = 0.80, absolute), however, differ by almost a factor of 7. The fluorescence intensity increase caused by the matrix rigidity (rigidochromic effect) is well-understood,[33] which is largely due to the suppression of the fluorophore thermal decay (e.g., rotational, vibrational, collisional) in the excited state.

When the **SDM1** film is placed under N_2 or vacuum, the expected dual-emission from both intense blue fluorescence and strong green RTP can be observed (photos in Figure 3b). The green "after-glow" from the RTP suggests a decay lifetime on the order of subseconds. The steady-state emission under N_2 is red-shifted (by 1195 cm^{-1}) to 470 nm. With an instrument setup of a 50 ms delay, the RTP spectrum is separated from that of the total emission (Figure 3b). With a

DOI: 10.1021/acsami.5b04075
ACS Appl. Mater. Interfaces 2015, 7, 17209−17216

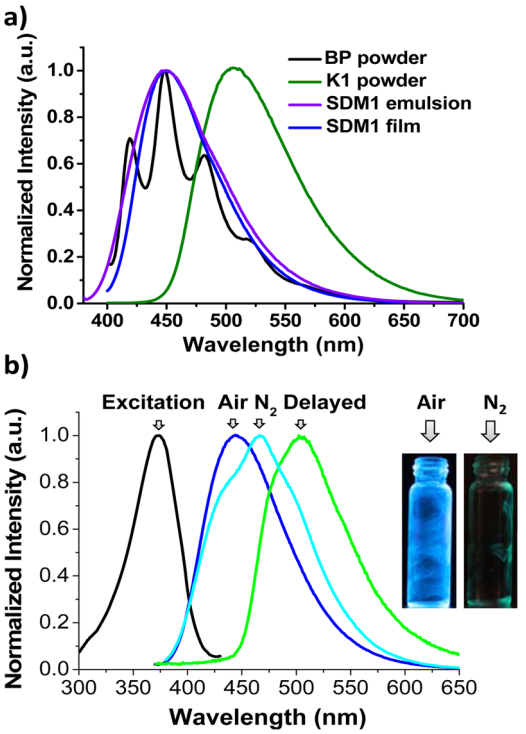

Figure 3. (a) Steady-state emission spectra of benzophenone (**BP**, blackline) powder, **K1** powder (green line), **SDM1** film (blue), and emulsion (purple) excited at 364 nm. (b) Steady-state excitation (black line) and emission spectra of **SDM1** thin film in air (blue line) and in N_2 (cyan line), and delayed emission of **SDM1** thin film under vacuum (Δt = 50 ms, λ_{ex} = 389 nm). Images showing that, when the **SDM1** thin film on the inner wall of a vial is exposed to the air, only blue fluorescence is observed under UV excitation from a hand-held lamp (λ_{ex} = 365 nm); when a stream of N_2 is blown into the vial, a green "after-glow" can be captured after the excitation has ceased.

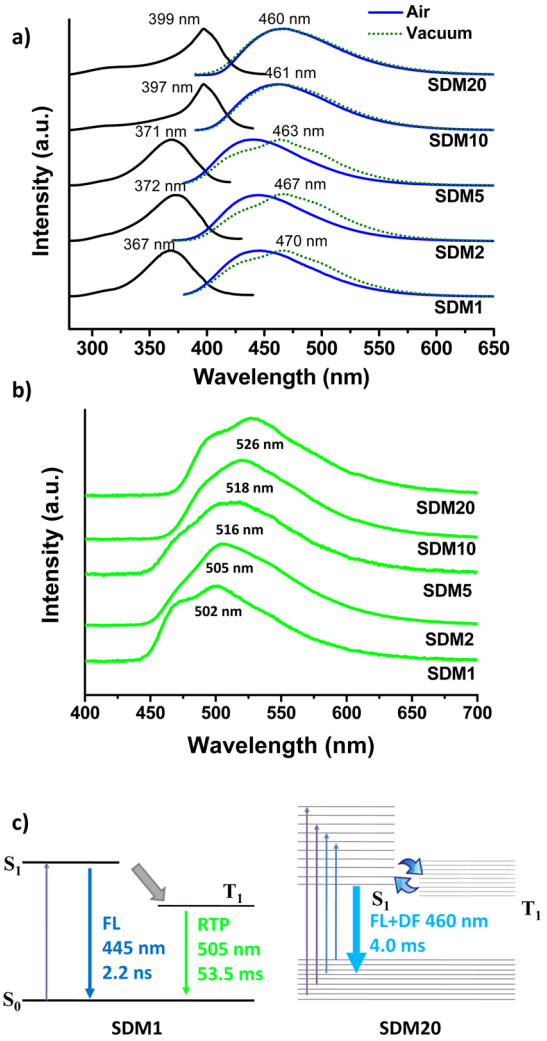

Figure 4. (a) Trend of steady-state excitation and emission spectra of **SDM1-SDM20** under air and vacuum at room temperature. The maximal values of excitation and emission spectra under vacuum are labeled (maximal values of emission spectra under air are shown in Table 2 due to space constraint). (b) Trend of delayed emission spectra of **SDM1-SDM20** thin films at 77 K (Δt = 50 ms, λ_{ex} = 365 nm). (c) Illustration of polymerization-enhanced intersystem crossing (PEX) with simplified Jablonski diagrams.

maximum at 505 nm (τ_{RTP} = 53.5 ms), the singlet−triplet energy gap ΔE_{ST} is estimated to be 2670 cm^{-1} or 7.6 kcal/mol, which is comparable to that of benzophenone (5.7 kcal/mol or 1995 cm^{-1}).[34] A suitable value of ΔE_{ST} can both enhance ISC and provides a necessary barrier to prevent total degeneracy of singlet and triplet states, thus giving rise to a wavelength-distinguishable dual emission.

The tunable features of the fluorescence and RTP of the SDMs through concentration effects were then studied. With the condensation polymerization, the weight content of **K1** can go up to 20% without showing any sign of phase separation based on the TG data (Figure 2). This is one of the biggest advantages compared to the previously reported dye-blend or dye-initiator systems.[15] In the case of the boron diketone−polylactide system, a minimum of ∼30 repeating units is required.[4] The spectral evolution of the SDM films with various **K1** contents is shown in Figure 4a. The steady-state emission spectra both under air and in vacuum were recorded at room temperature (the numerical values are shown in Table 2). For both excitation and emission under air, which is mainly fluorescence, the spectra progressively shift to the red regions (excitation from 367 → 399 nm and emission from 445 → 467 nm for **SDM1** to **SDM20**); the emission under vacuum, which is the total emission of fluorescence and RTP, however, exhibits an opposite trend of shifting (470 → 460 nm). It is apparent that the *fluorescence and RTP emission bands are merging.*

Table 2. Luminescence Characterization of the SDM Films at Room Temperature under Vacuum and at 77 K

	λ_{FL} (nm)[a]	τ_{FL} (ns)[b]	Φ_F (%)[c]	λ_{RTP} (nm)[d]	τ_{RTP} (ms)[e]	τ_{77K} (ms)[e]
SDM 1	445	2.2	80	505	53.5[g]	148
SDM2	446	2.2	71	502	60.9[g]	145
SDM5	441	2.3	54	500	70.2[g]	166
SDM10	460	*f*	25	463	9.8[h]	136
SDM20	460	*f*	18	460	4.0[h]	149

[a]Fluorescence emission maximum excited at excitation maxima. [b]Weight-averaged fluorescence lifetime. [c]Absolute emission quantum yields under air. [d]Room-temperature phosphorescence emission maximum excited at excitation maxima. [e]Pre-exponent weighted RTP lifetime at emission maxima. [f]A long-lived component trailing outside the measurement range in the fluorescence mode (range = 800 ns) and a fast component with a lifetime of 2.2 ns. [g]Emission wavelength is 500 nm. [h]Emission wavelength is 460 nm for the delayed fluorescence.

DOI: 10.1021/acsami.5b04075
ACS Appl. Mater. Interfaces 2015, 7, 17209−17216

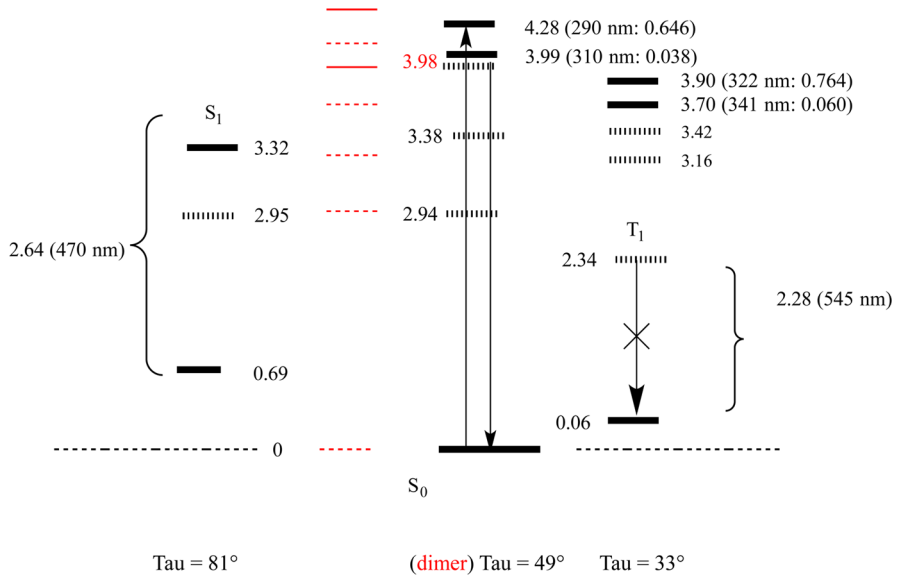

Figure 5. Calculated energy levels of representative singlet and triplet configurations shown in a simplified Jablonski diagram. Tau denotes the torsional angle between the two phenyl rings in **K1**.

At 77 K, however, the trend of phosphorescence appears to be backward: the delayed spectra are gradually red-shifting as the concentration of **K1** increase (Figure 4b). Since the delayed spectroscopic measurement at 77 K collects radiative decays from much less thermalized states compared to those at 298 K, the emission is largely from the lowest triplet states. As a result, the gradual red shift indicates that the lowest triplet states of the **K1** aggregates are also lower in energy compared to isolated **K1** molecules. The red-shift, similar to that observed for the singlet-state emission, is also ascribed to the excitonic interactions. This is clearly visible from Figure 4b, where the phosphorescence maxima are recorded to be 502, 505, 516, 518, and 526 nm, respectively for films **SDM1**-**SDM20**.

To explain the mergence of the two emission bands at room temperature, a graphic illustration is provided in Figure 4b: on the left for **SDM1**, largely monomeric **K1** is dual-emissive at a low concentration and exhibits two distinct emission bands corresponding to typical fluorescence (FL) and room-temperature phosphorescence (RTP), respectively; on the right for **SDM20**, elevated concentration of **K1** leads to aggregates and thus the formation of bandlike electronic states for the polymer due to excitonic splittings. The bandlike structure has a substantial overlap between the singlet and triplet manifolds; it is responsible for the decreased singlet−triplet energy gap and enhanced vibronic coupling, which thoroughly mixes these states and gives rise to a solo band comprising both fluorescence and back-populated fluorescence (delay fluorescence, DF).[35] The increased communication between singlet and triplet states as a function of **K1** concentration can also explain the lifetime measurements for the RTP (Table 2), that a sudden reduction in lifetime is noticed for **SDM10** (9.8 ms) and **SDM20** (4.0 ms). The reduction is very likely caused by these overlapping singlet−triplet energy bands, where back-population can lead to delayed fluorescence (DF) and drain more quickly the long-lived triplet states.[17] The lifetimes of the delayed emissions at 77 K, however, are all similar in scale (Table 2, 136−166 ms) irrespective of **K1** concentrations. The data suggest that the back-population pathway should be thermally activated and can be efficiently cut off at a lower temperature. The absence of the RTP in the pure **K1** solid, however, is ascribed to more active thermal decay pathways as a result of closer ground and triplet state energy gap in solids. Indeed, at 77 K, the delayed emission almost identical to that of the steady-state emission with a lifetime of 189 ms from the **K1** solid can be observed (Figure S3 and Table 2). In addition, the phosphorescence lifetimes for all SDMs at 77 K are similar since the thermally excited back-population pathway is hindered. Correspondingly, the nonthermally equilibrated emission spectra at 77 K show a red-shifting trend (opposite to that at room temperature) to the lower emissive triplet manifolds (Figure S3).

Finally, we performed theoretical calculations to gain more insight on how **K1** conformation as well as concentration influences the photophysical properties of the WPU polymers. All calculations were accomplished with Gaussian 09W64 software.[36] It has long been established that the phenyl rings in benzophenone's ground state are not coplanar, but twisted by ∼30−40°. It was already recognized by Hoffmann and Swensen[37] that the twist is reduced in the excited singlet S_1. In contrast, the phenyl rings in the S_1 state for 4-dimethyamino substituted benzophenone are almost perpendicular. The electron-donating character of the substituent and the reorientation of the phenyl rings explain several features of the spectra, namely the weak fluorescence and the striking red shift in absorption and emission relative to unsubstituted benzophenone.[38] Dual fluorescence in such systems is explained by effects of geometrical changes upon excitation, such as the "twist-induced intermolecular charge transfer" model and variants.[39]

We modeled chromophore **K1** with a density functional CAM-B3LYP[40] which incorporates a long-range correction. Such a correction can describe charge transfer transitions with reasonable accuracy.[41,42] The cc-pVDZ Dunning basis we chose promises reasonable structures and semiquantitative approximations to spectra.[43] Excited states are described by time-dependent density functional theory with the same functional and basis. The medium is described by the Tomasi polarized continuum model.[44]

Computed states of the isolated molecule, with the Tomasi solvent with the dielectric constant of diethyl ether (which is

DOI: 10.1021/acsami.5b04075
ACS Appl. Mater. Interfaces 2015, 7, 17209−17216

not expected to deviate too much from that of the WPU), are summarized in the Jablonski diagram (Figure 5). The computed absorption spectrum includes a weak transition at 310 nm and a stronger transition at 290 nm (Figure S7). These are mixed $n-\pi^*$ and $\pi-\pi^*$ states with charge-transfer character, shifted from gas phase values by interactions with the polar solvent. The gas phase computed values are 317 and 278 nm. Shifts are qualitatively consistent with those predicted for benzophenone in water as modeled by Georg, Koutinho, and Canuto.[45] The most nearly equivalent calculations are by Duan et al.,[39] who studied dimethylaminobenzophenone by TD-B3LYP and TD-MPW1-PW91. Geometry optimization calculations used the 6-31G (d) basis and excitation energy calculations used 6-311+G (2d,p). Representing the solvent acetonitrile by a Tomasi polarizable continuum, they found excitations at 3.37 eV (f = 0.45) and 3.83 eV (f = 0.03) with B3LYP and 3.53 eV (f = 0.48) and 3.92 (f = 0.03) with MPW1-PW91. Corresponding experimental values are 3.59 and 3.81 eV.[38]

The geometry optimized triplet state is placed by variational calculation only ~2.34 eV above the S_0 equilibrium energy, and the distortion on the 0 surface from S_0 to T_1 equilibrium structure costs only ~0.06 eV. We might expect easy passage from the first singlet excited state at 3.98 eV to an excited singlet of energy 3.90 eV at the T_1 geometry. This could be followed by rapid population of the T_1 state and its red emission, estimated to lie near 2.28 eV or 545 nm. From the calculations, the substituted phenyl ring twists almost perpendicular to the unsubstituted ring in S_1 (Figure S8). The NR_2-substituent can keep its nitrogen lone pair in conjugation with its ring, or one can imagine that the nitrogen lone pair to twist out of conjugation. We do not find a minimum in the latter case; the substituent spontaneously moves from the out-of-conjugation orientation to re-establish conjugation. For that structure we calculate a major Stokes shift of 1.35 eV and fluorescence at 2.64 eV (470 nm). The experimental Stokes shift for *N*,*N*-dimethylamino benzophenone in acetonitrile is about 1.53 eV (emission at 2.06 eV, 602 nm). Duan et al.[39] underestimate the shift seriously (0.60 and 0.54 eV in B3LYP and MPW1-PW91, respectively).

We also attempt to address the issue of the impact of increasing **K1** concentration from 1% to 20% from calculations. As Table 2 shows, the intrinsic lifetime of fluorescence is increased and the characteristic time of room temperature phosphorescence shortens drastically as a function of increased **K1** concentration. This shortening is not observed at low temperature, so one can infer that a temperature-dependent process is producing phosphorescence at high concentrations. This must involve interactions between monomers of **K1** if we are to account for concentration effects. We assume that the motion made possible at high temperature allows a new pathway for slow emission. Since S_1 favors a huge conformational change which may be impeded in the solid, we may assume that the emission at low temperature passes primarily through S_1's vertically excited nonequilibrium geometry retained from the S_0 state, which is so similar to the T_1 equilibrium geometry. Direct passage to the triplet manifold does not require a major conformational change. At high temperature, the conformational change can occur, the new path through twisted S_1 is accessible. We call this the "blue" path since emission is at about 470 nm as compared with the emission from the triplet at about 540 nm. We modeled aggregation effects by considering a dimer of K1, separated by 3.5 and 7 Å. Aggregation seems to favor passage through twisted S_1, by lowering the S_1 vertical excitation energy and broadening the S_1 band; at a separation of 3.5 Å, the bandwidth for S_1 is about 0.05 eV. An attendant feature seems to be the production of triplet states which may open additional channels to the "blue" path. The calculations are consistent with the experimental observation that spectroscopic broadening and red shifts in concentrated samples could be noted.

In a recent communication, we proposed a model based on Kasha's exciton theory,[35] polymerization-enhanced intersystem crossing (PEX),[16] backed by theoretical calculations and ultrafast spectroscopy, to account for significant increased lifetimes for a luminescent organoboron polymer (vs monomer). Nonetheless, the calculated 250 ns for the intrinsic lifetime of the polymer excitons is on the borderline of fluorescence and phosphorescence in solution. The present system more convincingly demonstrates that the fluorescence and RTP states are indeed merging and causing more communications between the two states. Our studies[6,16] along with two previous reports by Fraser et al.,[4,46] point to a more general feature of possibly all dual-emissive systems for coupling emissive singlet and triplet excited states: *increased intermolecular interactions may lead to merging fluorescence and RTP bands* in suitable media. This can be a facile yet powerful way for tuning the emissive properties of polymeric materials without undergoing complicated chemical modifications.

CONCLUSIONS

In conclusion, we incorporated a benzophenone-based dye into a waterborne polyurethane system and obtained a series of single-component dual-emissive materials (SDMs) with both fluorescence and room-temperature phosphorescence. These luminescence properties of the SDMs can be tuned via the concentration of the dye as a result of enhanced singlet−triplet communications. With increasing dye loadings, we observed that the energy levels between singlet and triplet excited states are decreased, which results in enhanced communications between the two states. To back our model, we performed theoretical calculations and found that the presence of **K1** aggregates indeed channels singlet excited states onto the triplet states more easily. The method serves as a convenient way for tuning the luminescence properties of the WPU-based SDM system. We expect that the dye-concentration effects are a general feature for all SDM systems and more examples, including a water-soluble SDM system, will be presented in future reports.

ASSOCIATED CONTENT

Supporting Information

Synthetic details, characterization methods and steady-state emission spectra, excitation spectra, NMR spectra, particle-size distribution, low-temperature spectra, and theoretical calculations. The Supporting Information is available free of charge on the ACS Publications website at DOI: 10.1021/acsami.5b04075.

AUTHOR INFORMATION

Corresponding Authors

*E-mail: zxym@ustc.edu.cn (X.Z.).
*E-mail: gzhang@ustc.edu.cn (G.Z.).

Notes

The authors declare no competing financial interest.

DOI: 10.1021/acsami.5b04075
ACS Appl. Mater. Interfaces 2015, 7, 17209−17216

■ ACKNOWLEDGMENTS

The authors are grateful for financial support from National Natural Science Foundation of China (NSFC, 21222405 to G. Z. and 51073144 to X. Z.) and the National High Technology Research and Development Program of China (No. 2015AA033903 to X. Z.). We also thank Prof. J. N. Demas (University of Virginia) for his helpful discussion. For support, C. T. thanks the Body Foundation for support of travel and computing equipment, and Y. T. acknowledges support from BABKO, the research fund for Marmara University.

■ REFERENCES

(1) Hirata, S.; Totani, K.; Zhang, J.; Yamashita, T.; Kaji, H.; Marder, S. R.; Watanabe, T.; Adachi, C. Efficient Persistent Room Temperature Phosphorescence in Organic Amorphous Materials under Ambient Conditions. *Adv. Funct. Mater.* **2013**, *23*, 3386−3397.

(2) An, Z.; Zheng, C.; Tao, Y.; Chen, R.; Shi, H.; Chen, T.; Wang, Z.; Li, H.; Deng, R.; Liu, X.; Huang, W. Stabilizing Triplet Excited States for Ultralong Organic Phosphorescence. *Nat. Mater.* **2015**, *14*, 685−690.

(3) Cao, Y.; Koo, Y. E. L.; Kopelman, R. Poly (Decyl Methacrylate)-Based Fluorescent PEBBLE Swarm Nanosensors for Measuring Dissolved Oxygen in Biosamples. *Analyst* **2004**, *129*, 745−750.

(4) Zhang, G.; Palmer, G. M.; Dewhirst, M. W.; Fraser, C. L. A Dual-Emissive-Materials Design Concept Enables Tumour Hypoxia Imaging. *Nat. Mater.* **2009**, *8*, 747−751.

(5) Wang, X. D.; Gorris, H. H.; Stolwijk, J. A.; Meier, R. J.; Groegel, D. B.; Wegener, J.; Wolfbeis, O. S. Self-referenced RGB Colour Imaging of Intracellular Oxygen. *Chem. Sci.* **2011**, *2*, 901−906.

(6) Zhang, X.; Xie, T.; Cui, M.; Yang, L.; Sun, X.; Jiang, J.; Zhang, G. General Design Strategy for Aromatic Ketone-Based Single-Component Dual-Emissive Materials. *ACS Appl. Mater. Interfaces* **2014**, *6*, 2279−2284.

(7) Borisov, S. M.; Fischer, R.; Saf, R.; Klimant, I. Exceptional Oxygen Sensing Properties of New Blue Light-Excitable Highly Luminescent Europium (III) and Gadolinium (III) Complexes. *Adv. Funct. Mater.* **2014**, *24*, 6548−6560.

(8) Lehner, P.; Staudinger, C.; Borisov, S. M.; Klimant, I. Ultrasensitive Optical Oxygen Sensors for Characterization of Nearly Anoxic Systems. *Nat. Commun.* **2014**, *5*, 4460.

(9) Wang, X.; Wolfbeis, O. S. Optical Methods for Sensing and Imaging Oxygen: Materials, Spectroscopies and Applications. *Chem. Soc. Rev.* **2014**, *43*, 3666−3761.

(10) Lee, D.; Bolton, O.; Kim, B. C.; Youk, J. H.; Takayama, S.; Kim, J. Room temperature Phosphorescence of Metal-Free Organic Materials in Amorphous Polymer Matrices. *J. Am. Chem. Soc.* **2013**, *135*, 6325−6329.

(11) Bolton, O.; Lee, K.; Kim, H. J.; Lin, K. Y.; Kim, J. Activating Efficient Phosphorescence from Purely Organic Materials by Crystal Design. *Nat. Chem.* **2011**, *3*, 205−210.

(12) Yuan, W.; Shen, X.; Zhao, H.; Lam, J.; Tang, L.; Lu, P.; Wang, C.; Liu, Y.; Wang, Z.; Zheng, Q.; Sun, J.; Ma, Y.; Tang, B. Crystallization-Induced Phosphorescence of Pure Organic Luminogens at Room Temperature. *J. Phys. Chem. C* **2010**, *114*, 6090−6099.

(13) Xie, Z.; Chen, C.; Xu, S.; Li, J.; Zhang, Y.; Liu, S.; Xu, J.; Chi, Z. White-Light Emission Strategy of a Single Organic Compound with Aggregation-Induced Emission and Delayed Fluorescence Properties. *Angew. Chem., Int. Ed.* **2015**, *54*, 7181−7184.

(14) Lee, S. Y.; Yasuda, T.; Yang, Y. S.; Zhang, Q.; Adachi, C. Luminous Butterflies: Efficient Exciton Harvesting by Benzophenone Derivatives for Full-Color Delayed Fluorescence OLEDs. *Angew. Chem.* **2014**, *126*, 6520−6524.

(15) Zhang, G.; Xu, S.; Zestos, A. G.; Evans, R. E.; Lu, J.; Fraser, C. L. An Easy Method to Monitor Lactide Polymerization with a Boron Fluorescent Probe. *ACS Appl. Mater. Interfaces* **2010**, *2*, 3069−3074.

(16) Sun, X.; Wang, X.; Li, X.; Ge, J.; Zhang, Q.; Jiang, J.; Zhang, G. Polymerization-Enhanced Intersystem Crossing: New Strategy to Achieve Long-Lived Excitons. *Macromol. Rapid Commun.* **2015**, *36*, 298−303.

(17) Zhang, G.; Chen, J.; Payne, S. J.; Kooi, S. E.; Demas, J. N.; Fraser, C. L. Multi-Emissive Difluoroboron Dibenzoylmethane Polylactide Exhibiting Intense Fluorescence and Oxygen-Sensitive Room-Temperature Phosphorescence. *J. Am. Chem. Soc.* **2007**, *129*, 8942−8943.

(18) Zhang, G.; Fiore, G. L.; St. Clair, T. L.; Fraser, C. L. Difluoroboron Dibenzoylmethane PCL-PLA Block Copolymers: Matrix Effects on Room Temperature Phosphorescence. *Macromolecules* **2009**, *42*, 3162−3169.

(19) Zhang, G.; Evans, R. E.; Campbell, K. A.; Fraser, C. L. Role of Boron in the Polymer Chemistry and Photophysical Properties of Difluoroboron− Dibenzoylmethane Polylactide. *Macromolecules* **2009**, *42*, 8627−8633.

(20) Zhang, G.; St. Clair, T. L.; Fraser, C. L. Synthesis and Fluorescent Properties of Difluoroboron Dibenzoylmethane Polycaprolactone. *Macromolecules* **2009**, *42*, 3092−3097.

(21) You, Y.; Kim, S. H.; Jung, H. K.; Park, S. Y. Blue Electrophosphorescence from Iridium Complex Covalently Bonded to the Poly (9-Dodecyl-3-Vinylcarbazole): Suppressed Phase Segregation and Enhanced Energy Transfer. *Macromolecules* **2006**, *39*, 349−356.

(22) Ott, C.; Ulbricht, C.; Hoogenboom, R.; Schubert, U. S. Metallo-Supramolecular Materials Based on Amine-Grafting Onto Polypentafluorostyrene. *Macromol. Rapid Commun.* **2012**, *33*, 556−561.

(23) Kim, B. K.; Lee, Y. M. Polyurethane Ionomers from Cycloaliphatic Diisocyanate and Polytetramethylene Glycol. *J. Macromol. Sci., Part A: Pure Appl.Chem.* **1992**, *A29*, 1207−1221.

(24) Lee, J. S.; Kim, B. K. Poly(Urethane) Cationomers from Poly(Propylene) Glycol and Isophorone Diisocyanate - Emulsion Characteristics and Tensile Properties of Cast Films. *Prog. Org. Coat.* **1995**, *25*, 311−318.

(25) Cheong, I. W.; Nomura, M.; Kim, J. H. Synthesis and Aqueous Solution Behavior of Water-Soluble Polyurethane (IPDI-PPG-DMPA) Resin. *Macromol. Chem. Phys.* **2000**, *201*, 2221−2227.

(26) Pfister, A.; Zhang, G.; Zareno, J.; Horwitz, A. F.; Fraser, C. L. Boron polylactide Nanoparticles Exhibiting Fluorescence and Phosphorescence in Aqueous Medium. *ACS Nano* **2008**, *2*, 1252−1258.

(27) Kersey, F. R.; Zhang, G.; Palmer, G. M.; Dewhirst, M. W.; Fraser, C. L. Stereocomplexed Poly (Lactic Acid)− Poly (Ethylene Glycol) Nanoparticles with Dual-Emissive Boron Dyes for Tumor Accumulation. *ACS Nano* **2010**, *4*, 4989−4996.

(28) Chen, X.; Zhang, X.; Zhang, G. Wide-range Thermochromic Luminescence of Organoboronium Complexes. *Chem. Commun.* **2015**, *51*, 161−163.

(29) Bai, C.; Zhang, X.; Dai, J.; Li, W. A New UV Curable Waterborne Polyurethane: Effect of C═C Content on the Film Properties. *Prog. Org. Coat.* **2006**, *55*, 291−295.

(30) Wen, T. C.; Wang, Y. J.; Cheng, T. T.; Yang, C. H. The Effect of DMPA Units on Ionic Conductivity of EG−DMPA−IPDI Waterborne Polyurethane as Single-Ion Electrolytes. *Polymer* **1999**, *40*, 3979−3988.

(31) Seymour, R. W.; Cooper, S. L. Thermal-Analysis of Polyurethane Block Polymers. *Macromolecules* **1973**, *6*, 48−53.

(32) Grabowski, Z. R.; Rotkiewicz, K.; Rettig, W. Structural Changes Accompanying Intramolecular Electron Transfer: Focus on Twisted Intramolecular Charge-Transfer States and Structures. *Chem. Rev.* **2003**, *103*, 3899−4032.

(33) Loutfy, R. O. High-conversion Polymerization of Fluorescence Probes. 1. Polymerization of Methyl Methacrylate. *Macromolecules* **1981**, *14*, 270−275.

(34) Bush, G. E.; Rentzepis, P. M.; Jortner, J. Energy Decay Characteristics of Benzophenone. *J. Chem. Phys.* **1972**, *56*, 361−370.

(35) Kasha, M. Energy Transfer Mechanisms and the Molecular Exciton Model for Molecular Aggregates. *Radiat. Res.* **1963**, *20*, 55−70.

(36) Frisch, M. J.; Trucks, G. W.; Schlegel, H. B.; Scuseria, G. E.; Robb, M. A.; Cheeseman, J. R.; Scalmani, G.; Barone, V.; Mennucci,

DOI: 10.1021/acsami.5b04075
ACS Appl. Mater. Interfaces 2015, 7, 17209−17216

B.; Petersson, G. A.; Nakatsuji, H.; Caricato, M.; Li, X.; Hratchian, H. P.; Izmaylov, A. F.; Bloino, J.; Zheng, G.; Sonnenberg, J. L.; Hada, M.; Ehara, M.; Toyota, K.; Fukuda, R.; Hasegawa, J.; Ishida, M.; Nakajima, T.; Honda, Y.; Kitao, O.; Nakai, H.; Vreven, T.; Montgomery, J. A., Jr.; Peralta, J. E.; Ogliaro, F.; Bearpark, M.; Heyd, J. J.; Brothers, E.; Kudin, K. N.; Staroverov, V. N.; Kobayashi, R.; Normand, J.; Raghavachari, K.; Rendell, A.; Burant, J. C.; Iyengar, S. S.; Tomasi, J.; Cossi, M.; Rega, N.; Millam, J. M.; Klene, M.; Knox, J. E.; Cross, J. B.; Bakken, V.; Adamo, C.; Jaramillo, J.; Gomperts, R.; Stratmann, R. E.; Yazyev, O.; Austin, A. J.; Cammi, R.; Pomelli, C.; Ochterski, J. W.; Martin, R. L.; Morokuma, K.; Zakrzewski, V. G.; Voth, G. A.; Salvador, P.; Dannenberg, J. J.; Dapprich, S.; Daniels, A. D.; Farkas, Ö.; Foresman, J. B.; Ortiz, J. V.; Cioslowski, J.; Fox, D. J. *Gaussian 09*, Revision D.01; Gaussian, Inc.: Wallingford CT, 2009.

(37) Hoffmann, R.; Swenson, J. R. Ground-and Excited-State Geometries of Benzophenone. *J. Phys. Chem.* **1970**, *74*, 415−420.

(38) Singh, A. K.; Ramakrishna, G.; Ghosh, H. N.; Palit, D. K. Photophysics and Ultrafast Relaxation Dynamics of the Excited States of Dimethylaminobenzophenone. *J. Phys. Chem. A* **2004**, *108*, 2583−2597.

(39) Duan, X. H.; Li, X. Y.; He, R. X.; Cheng, X. M. Time-Dependent Density Functional Theory Study on Intramolecular Charge Transfer and Solvent Effect of Dimethylaminobenzophenone. *J. Chem. Phys.* **2005**, *122*, 084314.

(40) Yanai, T.; Tew, D. P.; Handy, N. C. A New Hybrid Exchange−Correlation Functional Using the Coulomb-Attenuating Method (CAM-B3LYP). *Chem. Phys. Lett.* **2004**, *393*, 51−57.

(41) Kobayashi, R.; Amos, R. D. The Application of CAM-B3LYP to the Charge-Transfer Band Problem of the Zincbacteriochlorin−Bacteriochlorin Complex. *Chem. Phys. Lett.* **2006**, *420*, 106−109.

(42) Mikołajczyk, M. M.; Zaleśny, R.; Czyżnikowska, Ż.; Toman, P.; Leszczynski, J.; Bartkowiak, W. Long-Range Corrected DFT Calculations of Charge-Transfer Integrals in Model Metal-free Phthalocyanine Complexes. *J. Mol. Model.* **2011**, *17*, 2143−2149.

(43) Dunning, T. H., Jr Gaussian Basis Sets for Use in Correlated Molecular Calculations. I. The Atoms Boron Through Neon and Hydrogen. *J. Chem. Phys.* **1989**, *90*, 1007−1023.

(44) Tomasi, J.; Mennucci, B.; Cammi, R. Quantum Mechanical Continuum Solvation Models. *Chem. Rev.* **2005**, *105*, 2999−3094.

(45) Georg, H. C.; Coutinho, K.; Canuto, S. Solvent Effects on the UV-visible Absorption Spectrum of Benzophenone in Water: A Combined Monte Carlo Quantum Mechanics Study Including Solute Polarization. *J. Chem. Phys.* **2007**, *126*, 034507.

(46) Zhang, G.; Kooi, S. E.; Demas, J. N.; Fraser, C. L. Emission Color Tuning with Polymer Molecular Weight for Difluoroboron Dibenzoylmethane-Polylactide. *Adv. Mater.* **2008**, *20*, 2099−2104.

DOI: 10.1021/acsami.5b04075
ACS Appl. Mater. Interfaces 2015, 7, 17209−17216